Front. Earth Sci. 2015, 9(2): 276–285
DOI 10.1007/s11707-014-0459-2

RESEARCH ARTICLE

Understanding the effects of the impervious surfaces pattern on land surface temperature in an urban area

Qin NIE (✉)[1], Jianhua XU[2]

1 Department of Spatial Information Science and Engineering, Xiamen University of Technology, Xiamen 361024, China
2 The Research Center for East-West Cooperation in China, The Key Laboratory of GIScience of the Ministry of Education of China, East China Normal University, Shanghai 200241, China

Abstract It is well known that urban impervious surface (IS) has a warming effect on urban land surface temperature (LST). However, the influence of an IS's structure, components, and spatial distribution on LST has rarely been quantitatively studied within strictly urban areas. Using ETM+ remote sensing images from the downtown area of Shanghai, China in 2010, this study characterized and quantified the influence of the IS spatial pattern on LST by selecting the percent cover of each IS cover feature and ten configuration metrics. The IS fraction was estimated by linear spectral mixture analysis (LSMA), and LST was retrieved using a mono-window algorithm. The results indicate that high fraction IS cover features account for the majority of the study area. The high fraction IS cover features are widely distributed and concentrated in groups, which is similar with that of high temperature zones. Both the percent composition and the configuration of IS cover features greatly affect the magnitude of LST, but the percent composition is a more important factor in determining LST than the configuration of those features. The significances and effects of the given configuration variables on LST vary greatly among IS cover features.

Keywords urban impervious surfaces, land surface temperature, spatial pattern, Shanghai city

1 Introduction

Recent estimates indicate that more than 50% of the world human population lives in urban areas (United Nations, 2006). Urbanization has become the most significant human activity process since the 20th century. Rapid urbanization changes land cover types from permeable land to anthropogenic impervious surfaces (IS) (Meiyappan and Jain, 2012). Urban IS have a higher solar radiation absorption, a greater thermal conductivity and capacity for releasing heat stored during the day and night. Therefore, a well-documented consequence of the growth in IS area due to urbanization is the formation of an urban heat island (UHI) that is a major component of urban climate. With the development of airborne or satellite thermal infrared remote sensing, urban IS can be estimated using remote sensing technology (Slonecker et al., 2001; Weng, 2012), and the surface UHI is typically characterized as urban land surface temperature (LST) (Hope et al. 2005).The relationship between IS and LST has become increasingly important as the urban IS continue to increase and has attracted great attention from scholars at home and abroad.

A large number of studies have sought to elucidate the relationship between IS and LST, which might be summarized into three aspects: qualitative description and comparison based on spatial distribution of IS and LST (Xiao et al., 2007); quantitative statistical analysis based on random sampling methods (Yang et al., 2005; Weng et al., 2007; Xian et al., 2007; Yuan et al., 2007; Zhang et al., 2009a); and studies of the scale effects of their relationship (Yue, 2005; Meng, 2010). These studies have contributed to the understanding of the relationship between urban IS and LST, but most of them so far only focus on the quantitative relationship between them, without taking spatial pattern into account. The current understanding of the relationship between IS and LST is far from complete.

In urban areas, the composition and structure of urban canopies are crucial factors influencing LST. Despite the increasing interest in the relationship between LST and urban materials and landscape compositions, especially between LST and vegetation abundance (Weng et al., 2004; Wong and Yu, 2005; Zhang et al., 2009b), a critical area remains poorly understand. It is well known that urban IS has a warming effect on LST. However, the influence of different types of IS structures, components, and spatial

Received November 19, 2013; accepted March 12, 2014

E-mail: nieqinhongyi@163.com

distributions on LST has rarely been quantitatively studied within strictly urban areas, where IS has clearly dominated the major urban land cover types. Different types of IS can be quantitatively determined by implementing sub-pixel percent imperviousness estimation and selecting certain threshold values of percent IS (Lu and Weng, 2006).

This study aims to quantify the influence of an IS spatial pattern on LST using the Landsat Enhanced Thematic Mapper Plus (ETM+) data from the downtown area of Shanghai City, China. The pixel-based IS fraction is estimated using the technique of linear spectral mixture analysis (LSMA) and LST is retrieved using the mono-window algorithm. Eight kinds of IS cover features are then obtained according to the magnitude of IS fractions in the study area, and a series of landscape metrics are selected to characterize and quantify the spatial patterns of each IS cover feature. At last, the quantitative relationships between LST and composition and configuration of IS cover features are examined.

2 Methods and data

2.1 Study area

The downtown area of Shanghai, China, located within the outer ring road (Fig. 1), has been chosen as the study area. Shanghai is the largest economic center of China, with a registered population of 23.03 million in 2010 and a total area of 6,340.5 km^2. Since the economic reform in 1978, it has experienced accelerated urbanization, with an urbanization rate (the ratio of urban population to total population) increasing from 59% in 1978 to 86% in 2007 (Yue et al., 2012). Consequently, its urban land cover has undergone significant changes, and the natural land cover has been changed into anthropogenic IS, especially within the outer ring road, the core urban area. Meanwhile, it has witnessed a severe urban thermal environment with accelerated urbanization. UHI effects have been detected in the downtown area since the early 1980s (Zhou and Zhang, 1982), the 1990s (Ding et al., 2002) and 2008 (Yue et al., 2012).

Since the early 1990s, urban planning has matured as the city develops in Metropolitan Shanghai. Some decision-making factors have encouraged Shanghai to develop more rationally than other cities in China. Therefore, detecting the relationship between IS and the urban thermal environment and evaluating the environmental influences of urban IS spatial pattern on LST is important in understanding, controlling, and planning the urban ecosystem.

2.2 Data

A cloud-free Landsat ETM+ image acquired in 2010 served as the primary data source for retrieving IS and LST

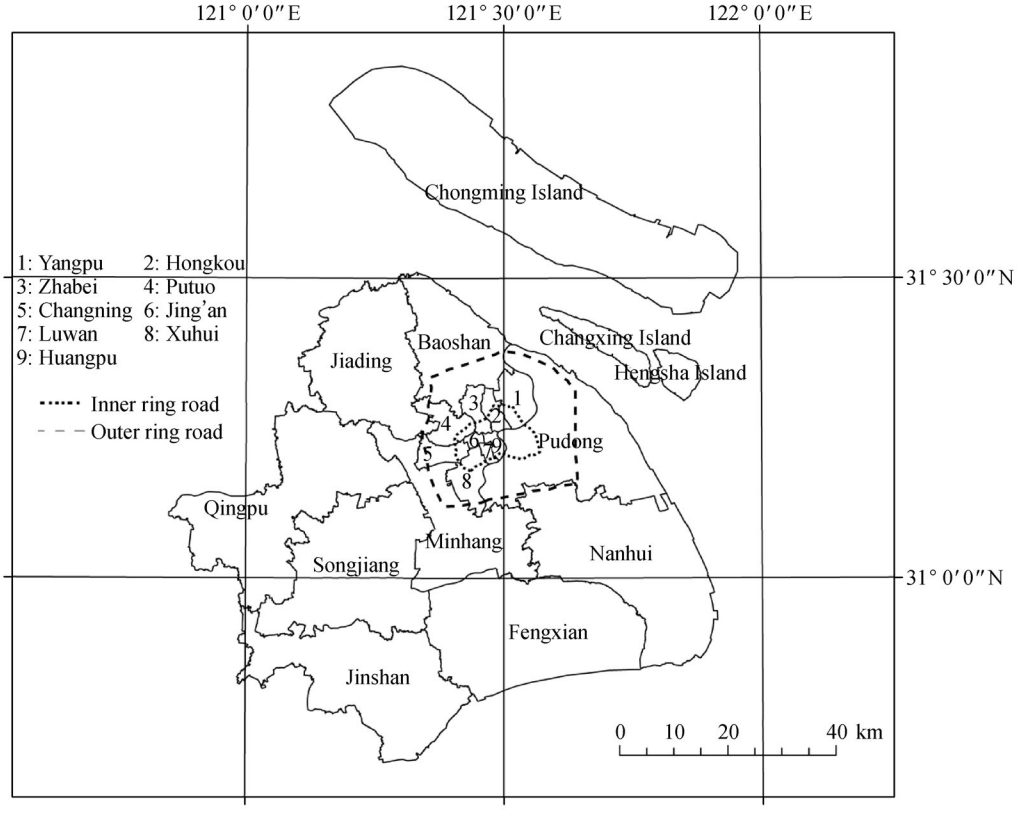

Fig. 1 The map of study area

in the study area. The image was registered to 1:10,000 topographic maps of Shanghai. It was assumed that the atmospheric conditions within the study area were homogeneous. So no atmospheric corrections were performed. The image was then further rectified to a Shanghai coordinate system (a modified Transverse Mercator coordinate system), and was re-sampled using the nearest neighbor algorithm with a pixel size of 60 m $\times$60 m for all bands (the same as the thermal band). The resultant root mean square (RMS) values were found to be less than 0.5 pixels.

2.3 Estimation of IS

The IS fraction was obtained by LSMA. Based on Ridd's (1995) vegetation-impervious surface-soil (V-I-S) model, the spectrum measured by a sensor is a linear combination of the spectra of all components (endmembers) within a pixel. A typical LSMA model can be expressed as (Small, 2001):

$$R_i = \sum_{k=1}^{n} f_k R_{ik} + ER_i, \quad (1)$$

where i is the number of spectral bands; k is the number of endmembers, in this research, $k = 3$; R_i is the spectral reflectance of band i containing all endmembers; f_k is the proportion of endmember k within the pixel; R_{ik} is the known spectral reflectance of endmember k within the pixel on band i; ER_i is the error for band i.

A constrained least-squares solution was used in this study, assuming that the following two conditions are simultaneously satisfied (Small, 2001):

$$\sum_{k=1}^{n} f_k = 1 \text{ and } 0 \leqslant f_k \leqslant 1. \quad (2)$$

Root Mean Square (RMS) error images were used to determine the overall error of all of the endmember abundance values for each pixel. A lower RMS error of the abundance images was desired.

$$\text{RMS} = \sqrt{\sum_{i=1}^{m} ER_i^2 / m}. \quad (3)$$

In this study, three endmembers, including vegetation (grass and trees), high-albedo (metal material, new concrete surface, sand, and some compound material), low-albedo (old concrete surface, cyan tile, and asphalt), were selected (Yue, 2009). A sum of high albedo and low albedo fractions was applied to obtain the IS fraction.

The accuracy assessment was conducted using two methods. The RMS for every image pixel was first calculated, which appears as noise and determines the overall error of all of the endmember abundance values for each pixel. The areas with high RMS error indicate low accuracy of spectral unmixing. Figure 2 illustrated the RMS frequency distribution and spatial image in 1997. As showed in Fig. 2, the RMS error values of less than 0.015 account for the majority of the pixels. The spatial distribution image of RMS error indicated that the IS fraction tended to be overestimated around the outer ring road. By linking to the corresponding aerial image, it was found that these regions were all high-albedo features, such as Shanghai Stadium, Hongkou Stadium, etc. The over-estimation of the IS fraction may be due to the building materials of these high-albedo features.

Secondly, a random sampling method was applied to assess the accuracy of IS estimation. The IS fraction of the samples was obtained from high resolution images. A sampling unit of 150 m$\times$150 m was used and 100 samples in the image were chosen. Figure 3 shows the difference between estimated values and actual values of IS fractions. The difference between estimation values and actual values is within $\pm$0.15. Overall, the results of IS fraction estimation are reliable.

2.4 Derivation of LST

The procedure described by Artis and Carnahan (1982) was adopted for retrieval of LST. The radiation correction

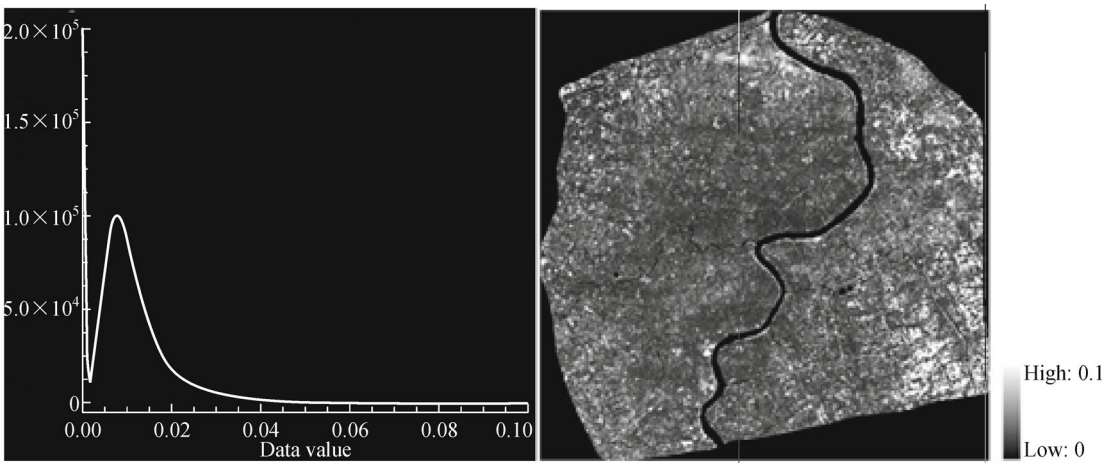

Fig. 2 The RMS frequency distribution and spatial image

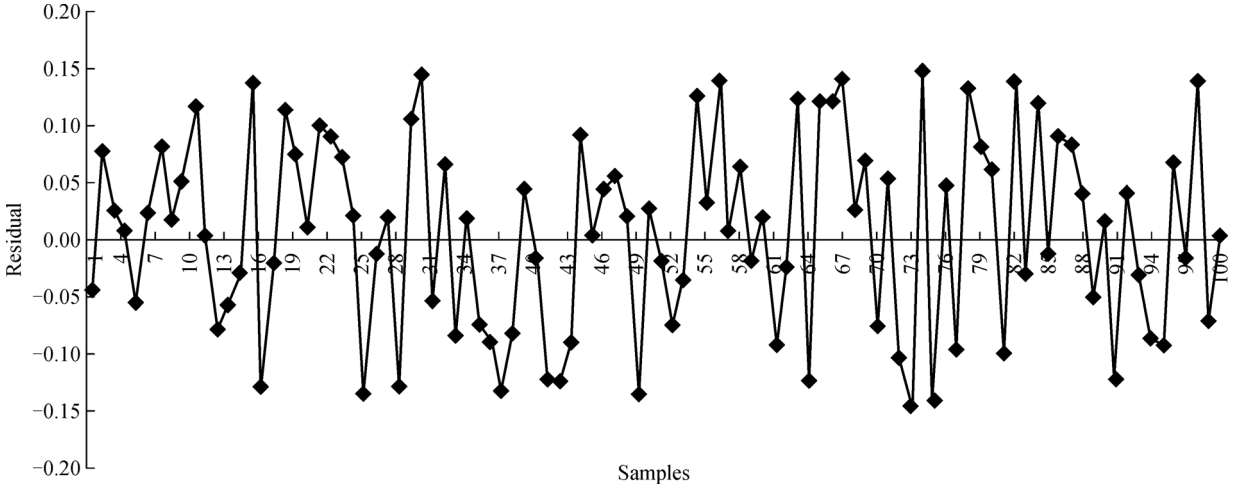

Fig. 3 The accuracy assessment of the impervious surface estimation

formula provided by the Landsat user manual was used to convert the digital number (DN) of the Landsat thermal band into spectral radiance:

$$L_\lambda = \text{gain} \times \text{DN} + \text{offset}, \tag{4}$$

where L_λ is at sensor radiance, gain is slope of the radiance/DN conversion function, and offset is the intercept of the radiance/DN conversion function. Gain and offset values are supplied in the metadata accompanying each TM/ETM+ image.

The spectral radiance can be converted to a physically useful variable using the inverse of the Planck function. This is the effective at-satellite temperature of the viewed Earth-atmosphere system:

$$T_B = \frac{K_2}{\ln\left(\frac{K_1}{L_\lambda} + 1\right)}, \tag{5}$$

where T_B is the effective at-satellite temperature (K), L_λ is the spectral radiance, K_1 and K_2 are two calibration constants, which are supplied by the metadata of Landsat images. The temperature values obtained above were referenced to a black body, which is quite different from the properties of real objects. Therefore, a correction of spectral emissivity (ε) is a must.

Furthermore, the emissivity corrected surface temperature was computed as follows (Artis and Carnahan ,1982):

$$\text{LST} = \frac{T_B}{1 + \left(\lambda \times \frac{T_B}{\rho}\right) L N_\varepsilon}, \tag{6}$$

where λ (11.5 μm) is the wavelength of the emitted radiance, h is Planck's constant (6.626×10^{-34} Js), σ is the Boltzmann constant (1.38×10^{-23} J/K), $\rho = 1 \times c/\sigma$, c is the velocity of light (2.998×10^8 m/s), ε is land surface thermal emissivity. We used the NDVI (normalized difference vegetation index) threshold method to obtain thermal emissivity. Based on Van (1993), thermal emissivity is highly correlated with NDVI after logarithmic transformation, with a correlation coefficient of $R = 0.94$. Thus, Van (1993) proposed an empirical relationship:

$$\varepsilon = 1.0094 + 0.047 \times \ln \text{NDVI}. \tag{7}$$

The formula is suitable because NDVI is greater than 0.157. For the land surface where NDVI is less than 0.157, according to Gong et al. (2005), the emissivity was given a value of 0.923, and water body was given a value of 0.9925.

The LST values derived above are reliable. First, in the conversion from DN values into spectral radiance, the radiation correction formula provided by the Landsat user manual was applied. The results are reliable. During the conversion from spectral radiance into the effective at-satellite temperature, the calibration coefficients are also supplied by the metadata of Landsat images. Finally, the emissivity corrected surface temperature was computed based on the empirical formula of Van (1993) and Gong et al. (2005) that has been demonstrated by many researches.

2.5 Measures of the composition and configuration of IS spatial pattern

A series of metrics have been developed and successfully applied to characterize and quantify the composition and configuration of land cover features (Xu et al., 2001; McGarigal et al., 2002; Xu et al., 2003; Zhou et al., 2011). In this study, the most frequently used composition metric, the percent cover of each IS cover feature was used, which can be calculated by the area of each IS cover divided by the total area of the research area.

According to the potential effects on LST and application in urban landscape planning, ten configuration metrics were selected, including: 1) fragmentation indices: largest

patch index (LPI), patch density (PD), and edge density (ED); 2) patch area indices: mean and standard deviation of patch area (MNArea, SDArea); 3) patch shape indices: mean and standard deviation of patch shape index (MNShape,SDShape); 4) proximity metrics: mean and standard deviation of Euclidian nearest neighbor distance (MNEnn,SDEnn); 5) a connectivity metric: patch cohesion index (CI). In this study, the ten configuration variables of each IS cover feature were calculated, respectively.

2.6 Statistical analyses

In this study, re-sampling areas of 100×100 pixels were extracted randomly, and 100 sampling areas were selected in order to explore the effects of the IS spatial pattern on LST. For each re-sampling area, the percent cover and ten configuration metrics of each IS feature were calculated, and the mean LST was also summarized. On this basis, a Pearson correlation analysis was first used to examine the strength of bivariate associations between LST and the variables of composition and configuration of IS cover features:

$$r_{xy} = \frac{\sum_{i=1}^{n}(x_i-\overline{x})(y_i-\overline{y})}{\sqrt{\sum_{i=1}^{n}(x_i-\overline{x})^2}\sqrt{\sum_{i=1}^{n}(y_i-\overline{y})^2}}, \quad (8)$$

where n is the sample number; x_i represents the value of x for the sample i; y_i represents the value of y for the sample i; $\overline{x}$ is the mean for all x_i; $\overline{y}$ is the mean for all y_i. Testing for the significance of the correlation coefficient commonly employs the t distribution.

For the composition and configuration variables that passed the significance test, LST was then modeled as a linear function of all composition variables or a combination of all composition variables and configuration variables of a given IS cover feature. These regression models can investigate whether adding configuration variables could better predict LST, compared with only composition variables as independent variables.

The multiple linear regression model is

$$Y = a_0 + a_1x_1 + a_2x_2 + \cdots + a_nx_n, \quad (9)$$

where Y is the dependent variable (LST), a_i is the coefficient of the independent variables x_i (composition/configuration variables).

3 Results

3.1 Spatial pattern of IS and LST

The IS fraction, which is estimated within a continuous range of between 0% and 100%, was mapped for the study area. According to the magnitude of impervious surface fractions (ISF), there, eight IS types were designated as IS1 through IS8 (Fig. 4): IS1 (ISF < 30%), IS2 (30% ⩽ ISF < 40%), IS3 (40% ⩽ ISF < 50%), IS4 (50% ⩽ ISF < 60%), IS5 (60% ⩽ ISF < 70%), IS6 (70% ⩽ ISF < 80%), IS7 (80% ⩽ ISF < 90%), and IS8 (ISF ⩾ 90%). As illustrated in Fig. 4, the high fraction IS cover features predominate in the study area. Statistically, the IS6 accounts for 15.09% of the whole study area, IS7 accounts for 38.44%, and IS8 accounts for 33.15%. Only 13.32% of

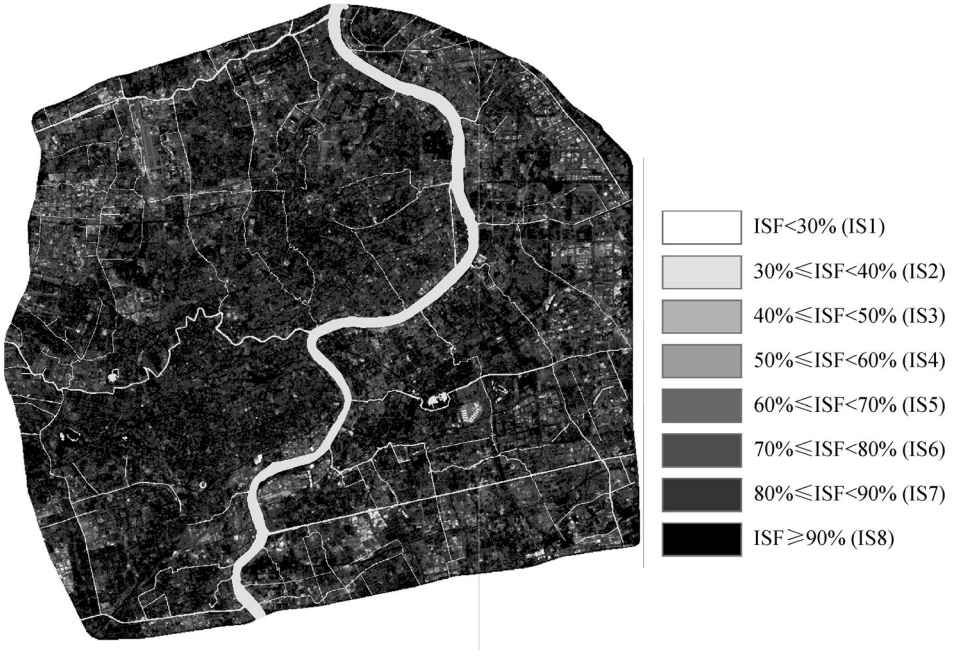

Fig. 4 The spatial pattern of IS cover features

the study area is covered with IS5 and below. The high fraction ISs (fraction greater than 70%) distribute widely and concentrate in groups.

On the other hand, as displayed in Fig. 5, the LST in the study area ranges from 279.238 K to 294 K, and the mean is 293.78 K. For the whole study area, the LST spatial distribution features appear to alternate with high and low temperature. The high temperature zones are widely distributed and concentrated in groups, which is a pattern similar to that of the high fraction IS areas, but the UHI is not prominent across the whole study area.

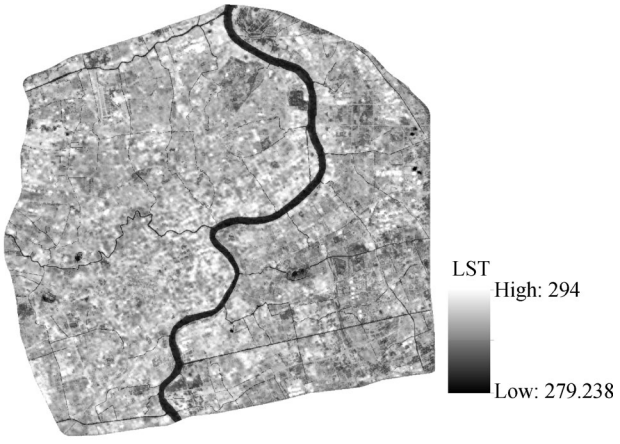

Fig. 5 The spatial pattern of LST

3.2 Effects of the composition of IS on LST

According to Table 1, all of the composition variables, except IS1, are significantly related to LST. Some variables such as percent of IS3, IS4, IS5, and IS6 have the strongest relationships with LST, with the Pearson correlation coefficients between 0.72 and 0.77. The percent cover of IS7 and IS8 has also relatively strong relationships with LST, with Pearson correlation coefficients between 0.58 and 0.6. Percent cover of IS2 is, however, weakly related to LST.

Based on the close LST-IS composition variables correlation revealed in the aforementioned studies, further investigations become necessary to interpret the LST dynamic responses to the changes in composition variables of IS cover and to establish quantitative relationships between them. This was done using a multivariate regression linear model (Table 2, model 1), with LST as the dependent variable and all composition variables passing the significance test as the independent variables.

The *F*-test indicates that the regression model (Table 2, model 1) is statistically significant at the 99% confidence level. Approximately 86.1% of the variation in LST can be explained jointly by the six composition variables of IS cover features, namely IS2, IS3, IS4, IS5, IS7, and IS8. All of these variables are significant at the 99% or 95% confidence level, except for percent cover of IS2.Three coefficients of percent cover of IS4, IS7, and IS8 are positive, suggesting that an increase in the percent cover of IS4, IS7, and IS8 will increase LST. In contrast, the negative coefficients of percent cover of IS3 and IS5 indicate that LST will decrease with the increase of relative abundances of IS3 and IS5.

3.3 Effects of the configuration of IS on LST

According to the Pearson correlation analysis (Table 1), some of the configuration variables show a significant bivariate relationship to LST. For IS5 and IS6, all 10 configuration variables show a significant bivariate relationship to LST, respectively. For IS3, IS4, IS7, and IS8, about seven or eight configuration variables show a significant bivariate correlation with LST, respectively. While only two configuration variables (i.e., patch density

Table 1 Pearson correlation coefficients between LST and variables of composition and configuration of IS cover features

		IS cover features							
		IS8	IS7	IS6	IS5	IS4	IS3	IS2	IS1
Composition	Percent cover	0.58**	0.6**	−0.77**	−0.76**	−0.72**	−0.74**	−0.24*	0.001
Configuration	PD	0.504**	0.26**	−0.61**	−0.76**	−0.7**	−0.78**	−0.31**	–
	LPI	0.02	0.37**	−0.51**	−0.62**	−0.6**	−0.43**	−0.09	–
	ED	0.73**	0.7**	−0.74**	−0.76**	−0.71**	−0.76**	−0.27*	–
	MNArea	0.14	−0.03	−0.78**	−0.45**	−0.36**	−0.29*	0.22	–
	SDArea	0.01	0.29*	−0.72**	−0.52**	−0.33**	−0.26*	−0.02	–
	MNShape	0.37**	−0.4**	−0.75**	−0.43**	−0.32**	−0.13	0.01	–
	SDShape	0.47**	0.175	−0.72**	−0.49**	−0.09	−0.27*	0.01	–
	MNEnn	−0.67**	−0.48**	0.69**	0.65**	0.22	0.41**	0.05	–
	SDEnn	−0.64**	−0.52**	0.51**	0.74**	0.45**	0.1	0.18	–
	CI	0.39**	0.29*	−0.69**	−0.36**	−0.26**	−0.31**	0.18	–

Notes: * Correlation is significant at the 0.05 level (two-tailed); ** Correlation is significant at the 0.01 level (two-tailed).

and edge density) are significantly correlated with LST for IS2. In addition, some of the configuration variables show as strong a bivariate relationship with LST as that of their corresponding composition variables. For example, the correlation coefficient of mean patch area (MNArea) of IS6 is close to that of percent cover of IS6, and the correlation coefficient between LST and patch density (PD) of IS5 is as strong as that of percent cover of IS5 with LST. However, in most cases, the Pearson correlation coefficients of configuration variables are smaller than that of their corresponding composition variables.

Taking a combination of all composition variables and configuration variables for a given IS cover that pass the significance test as independent variables, LST was modeled (model 2-model 8, Table 2). These multivariate regression linear models were established in order to investigate whether adding configuration variables could better predict LST, compared with only composition variables as independent variables. *F*-tests indicate that all of the regression models are statistically significant at the 95% confidence level. Results from these models suggested that although composition variables can explain well the variation in LST, a combination of composition and configuration variables better explains the variation. Many of the configuration variables can significantly add to the explanation of LST.

For IS2, only two configuration variables, i.e., patch density (PD) and edge density (ED) are significantly correlated to LST in the bivariate correlation analysis (Table 1), and the correlations are both stronger than that of the composition variable to LST. Approximately 86% of the variation in LST is explained jointly by the six composition variables and IS1 configuration variables (model 2, Table 2). After adjusting for the effects of composition variables, patch density and edge density lost significance.

For IS3, patch density, largest patch index, edge density, mean patch area, standard deviation of patch area, standard deviation of patch shape index, mean Euclidian nearest neighbor distance, and patch cohesion index are significantly correlated with LST in the bivariate correlation analysis. Patch density and edge density are relatively strongly correlated with LST. A combination of the six composition variables and IS3 configuration variables explain about 90.3% of the variation in LST (model 3, Table 2). After adjusting for the effects of composition, standard deviation of patch shape index and mean Euclidian nearest neighbor distance lost significance. Among the configuration variables remaining significant, patch density is the most important one. In addition, percent cover of IS3 and IS5 are no longer significant when adding the configuration variables of IS3. Largest patch index and cohesion index have a positive effect on LST, indicating that LST increases with the increase of IS3 largest patch index and cohesion index. Patch density, mean, and standard deviation of patch area have negative effects on LST, suggesting that LST decreases with the increase of IS3 patch density, mean, and standard deviation of patch area.

For IS4, all of the configuration variables are significantly correlated with LST in the bivariate correlation analysis, except standard deviation of patch shape index and mean Euclidian nearest neighbor distance (Table 1). Patch density and edge density are relatively strongly correlated with LST. A combination of the six composition variables and IS4 configuration variables explains about 89% of the variation in LST (Model 4, Table 2). After adjusting for the effects of composition, largest patch index and standard deviation of patch area remain significant. In addition, percent cover of IS4 and IS5 are no longer significant when adding the configuration variables of IS4. Largest patch index has a negative effect on LST, suggesting that LST decreases with the increase of IS4 largest patch index. LST, however, increases with the increase of standard deviation of patch area.

For IS5, all of the configuration variables are significantly correlated with LST in the bivariate correlation analysis. Patch density, edge density, and standard deviation of Euclidian nearest neighbor distance are relatively strongly correlated with LST (Table 1). A combination of the six composition variables and IS5 configuration variables explains about 92.2% of the variation in LST (Model 5, Table 2). After adjusting for the effects of composition, patch density, mean Euclidian nearest neighbor distance, and cohesion index remain significant, and these variables have a positive effect on LST. Furthermore, patch density is the most important. In addition, percent cover of IS2 and IS3 are no longer significant when adding the configuration variables of IS5.

For IS6, all of the configuration variables are significantly correlated with LST in the bivariate correlation analysis, and the correlations are strong with coefficients ranging from 0.51 to 0.78 (Table 1). Approximately 92% of the variation in LST is explained jointly by the five composition variables and IS6 configuration variables (Model 6, Table 2). After adjusting for the effects of composition, largest patch index, standard deviation of patch area and cohesion index still remain significant, and standard deviation of patch area is the most important. The positive coefficient of largest patch index and cohesion index indicate that LST increases when largest patch index increases and the IS6 surfaces are less fragmented, holding the IS cover composition constant. The negative coefficient of standard deviation of patch area indicates that LST increases with the decrease of the standard deviation of patch area.

For IS7, all of the configuration variables are significantly correlated with LST in the bivariate correlation analysis, except mean patch area and standard deviation of patch shape index. Edge density has a relatively strong correlation with LST, and the other IS7 configuration variables have a weak correlation with LST (Table 1).

Table 2 Linear regression models between LST and composition variables or the combination of composition and some configuration variables

Model 1		Model 2		Model 3		Model 4	
Cover feature	Coefficient	Cover feature	Coefficient	Cover feature	Coefficient	Cover feature	Coefficient
IS2	0.51 (0.11)	IS2	0.015 (0.003)	IS2	1.02* (0.22)	IS2	0.92* (0.2)
IS3	−0.86** (−0.45)	IS3	−1.03** (−0.53)	IS3	7.46 (3.84)	IS3	−1.2** (−0.62)
IS4	1.76** (2.66)	IS4	1.64** (2.47)	IS4	1.19** (1.79)	IS4	1.1 (1.66)
IS5	−0.22* (−1.1)	IS5	−0.39** (−1.89)	IS5	−0.01 (−0.05)	IS5	−0.17 (−0.84)
IS7	0.16** (1.08)	IS7	−0.16** (−1.9)	IS7	0.18** (1.23)	IS7	0.12** (0.84)
IS8	0.096** (1.73)	IS8	−0.06** (−1.11)	IS8	0.12** (2.14)	IS8	0.06* (0.99)
R^2	0.872 (0.861)	PD_IS2	−0.04 (−0.06)	PD_IS3	−1.17** (−4.1)	PD_IS4	0.13 (1.06)
		ED_IS2	0.03 (0.07)	LPI_IS3	7.93* (0.46)	LPI_IS4	−28.86** (−1.8)
		R^2	0.871 (0.86)	MNArea_IS3	−32.02** (−2.53)	MNArea_IS4	−8.37 (−0.39)
				SDArea_IS3	−14.52** (−2.21)	SDArea_IS4	19.65** (1.53)
				SDShape_IS3	1.66 (0.16)	MNShape_IS4	−7.35 (−0.19)
				MNEnn_IS3	−0.0001 (−0.15)	SDEnn_IS4	0 (.01)
				CI_IS3	0.1** (3.61)	CI_IS4	0.01 (0.2)
				R^2	0.92 (0.903)	R^2	0.91 (0.89)

Model 5		Model 6		Model 7		Model 8	
Cover feature	Coefficient	Cover feature	Coefficient	Cover feature	Coefficient	Cover feature	Coefficient
IS2	−0.33 (−0.07)	IS2	−0.39 (−0.09)	IS2	0.28 (0.06)	IS2	0.52 (0.11)
IS3	−0.26 (−0.13)	IS3	−0.09 (−0.05)	IS3	−1.08* (−5.6)	IS3	−1.49** (−0.77)
IS4	1.38** (2.08)	IS4	1.24** (1.87)	IS4	1.97** (2.97)	IS4	1.33** (2)
IS5	−1.36** (−6.7)	IS5	−0.08 (−0.42)	IS5	−0.42** (−0.83)	IS5	−0.24** (−1.2)
IS6	−0.08** (−0.96)	IS7	0.05** (0.37)	IS6	−0.07* (−0.83)	IS6	−0.16** (−1.9)
IS7	0.06** (0.38)	PD_IS6	−0.03 (−0.29)	IS7	0.1 (0.67)	IS7	−0.05 (−0.33)
PD_IS5	0.3** (4.72)	LPI_IS6	1.22** (1.49)	PD_IS7	0.01 (0.23)	PD_IS8	0.26** (1.66)
LPI_IS5	0.07 (0.02)	MNArea_IS6	−5.61 (−1.16)	LPI_IS7	−0.004 (−0.04)	ED_IS8	−0.04** (−2.87)
MNArea_IS5	4.89 (0.48)	SDArea_IS6	−3.76* (−2.69)	ED_IS7	−0.004 (−0.099)	MNShape_IS8	5.58** (0.47)
SDArea_IS5	−3.03 (−0.79)	MNShape_IS6	7.17 (0.53)	SDArea_P7	0.05 (0.16)	SDShape_IS8	5.47** (2.06)
MNShape_IS5	5.06 (0.21)	SDShape_IS6	−3 (−0.49)	MNShape_P7	0.02 (0.001)	MNEnn_IS8	−0.03 (−0.39)
SDShape_IS5	−4.61 (−0.47)	MNEnn_IS6	0.003 (0.05)	MNEnn_P7	0.005 (0.009)	SDEnn_IS8	0.02* (0.28)
MNEnn_IS5	0.018* (0.36)	SDEnn_IS6	0 (−0.17)	SDEnn_P7	−0.05 (−0.17)	CI_IS8	−0.15** (−0.71)
SDEnn_IS5	0 (−0.15)	CI_IS6	0.03* (0.71)	CI_IS7	−0.03 (−0.29)	R^2	0.957 (0.947)
CI_IS5	0.07** (1.56)	R^2	0.936 (0.92)	R^2	0.899 (0.874)		
R^2	0.938 (0.922)						

Notes: Standardized coefficients were included in the parentheses. * Correlation is significant at the 0.05 level (two-tailed). ** Correlation is significant at the 0.01 level (two-tailed).

Approximately 87.4% of the variation in LST is explained jointly by the six composition variables and IS7 configuration variables (Model 7, Table 2). After adjusting for the effects of composition, all IS7 configuration variables lost significance. In addition, percent cover of IS2 and IS7 is no longer significant when adding the configuration variables of IS7.

For IS8, all of the configuration variables are significantly correlated with LST in the bivariate correlation analysis, except largest patch index, mean, and standard deviation of patch shape area. LST has a strongest correlation with edge density (Table 1). Approximately 94.7% of the variation in LST was explained jointly by the six composition variables and IS8 configuration variables (Model 8, Table 2). After adjusting for the effects of composition, all IS8 configuration variables remain significant, except mean Euclidian nearest neighbor distance. The correlation coefficient indicates that LST increases with increase of patch density, mean patch area, standard deviation of patch shape index, and Euclidian nearest neighbor distance. However, LST decreases with the increase of edge density and less IS8 fragment.

4 Discussion

The aforementioned results indicate that the percent composition and configuration of IS cover features greatly affect the magnitude of LST. Furthermore, the percent composition of IS cover features is a more important factor in determining LST than the configuration of those features, especially for the IS3 type and above. For IS2, the composition and configuration variables have a weak relationship with LST. However, the IS1 percent composition is not significantly correlated to LST. This may be partly due to the very small proportion cover of these two types of features in our study area.

The configuration of IS cover features also significantly affects LST. This is because different types of IS cover features have different thermal heat capacity, reflectance, and roughness, which lead to the non-uniformity of energy exchange and transmission among IS cover features, thus affecting LST. For a fixed relative amount of IS cover features, different spatial arrangements of IS cover features can affect significantly the magnitude of LST, but different configuration variables have varying significances and effects on LST.

In this study, a surprising result was found in that some of the configuration variables are strongly correlated to LST in the bivariate correlation analysis, but are not significantly correlated to LST in the regression models. This is because configuration metrics are commonly correlated to composition metrics. So it is important to control the effects of composition while testing the effects of configuration of IS cover features on LST.

The results of this study not only can enhance the understanding of how LST varies with changing IS cover patterns but can also have an important realistic significance. The percent composition and configuration of IS cover features greatly affect the magnitude of LST, therefore, the impact of urbanization on UHI can be mitigated not only by balancing the relative amounts of IS cover features, but also by optimizing their spatial configuration. This provides important information to urban planners and natural resource managers on how to mitigate the impact of urbanization on UHI through scientific urban design. This is an important reference for ecological design and management, especially for areas where urbanization is still in process.

It is worthy of note that our study results are only based on LST data from one time point, and the research is conducted only for one metropolitan area. Future comparison research across metropolitan areas at different seasons, therefore, will be expected.

5 Conclusions

Using Landsat ETM+ data from the core urban area of Shanghai, China, this study quantified the influence of IS spatial pattern on LST. The percent cover of each IS cover feature and ten configuration metrics were selected to characterize and quantify the composition and configuration of IS cover features. The IS cover features with a fraction of greater than 70% account for about 86.68% of the study area, and they are widely distributed and concentrated in groups. LST spatial distribution features appear to alternate with high and low temperature. The high temperature zones show similar distribution characteristics with high fraction IS cover features. But the UHI is not prominent in the study area.

According to bivariate correlation analysis, all of the composition variables, except IS1, are significantly related to LST. The percent of IS3, IS4, IS5, and IS6 have the strongest relationships with LST, and the percent cover of IS7 and IS8 have also relatively strong relationships with LST. While the percent cover of IS2 is weakly related to LST. According to the regression model applied, approximately 86.1% of the variation in LST can be explained jointly by the six composition variables of IS cover features, i.e., IS2, IS3, IS4, IS5, IS7, and IS8.

Some of the configuration variables show a significant bivariate relationship to LST. But the Pearson correlation coefficients are smaller than those of their corresponding composition variables in most cases. Both the percent composition and configuration of IS cover features greatly affect the magnitude of LST, but the composition of IS cover features is a more important factor in determining LST than the configuration of those features, suggesting that the impact of urbanization on UHI can be mitigated not only by balancing the relative amounts of IS cover features, but also by optimizing their spatial configuration.

Acknowledgements This work was supported by the National Natural Science Foundation of China (Grant Nos. 41130525 and 41102224).

References

Artis D A, Carnahan W H (1982). Survey of emissivity variability in thermography of urban areas. Remote Sens Environ, 12(4): 313–329

Ding J C, Zhang Z K, Xi H, Zhou H M (2002). A study of the high temperature distribution and the heat island effect in the summer of the Shanghai area. Chin J Atmos Sci, 26(3): 412–420 (in Chinese)

Gong A D, Jiang Z X, Li J, Chen Y H, Hu H L (2005). Urban land surface temperature retrieval based on landsat TM remote sensing images in Beijing. Remote Sensing Information, (3): 18–20

Hope A, Engstrom R, Stow D (2005). Relationship between AVHRR surface temperature and NDVI in Arctic tundra ecosystems. Int J Remote Sens, 26(8): 1771–1776

Lu D, Weng Q (2006). Use of impervious surface in urban land-use classification. Remote Sens Environ, 102(1–2): 146–160

McGarigal K, Cushman S A, Neel M C, Ene E (2002). FRAGSTATS: Spatial Pattern Analysis Program for Categorical Maps. Computer software program produced by the authors at the University of Massachusetts, Amherst. Available at the following web site: http://www.umass.edu/landeco/research/fragstats/fragstats.html

Meiyappan P, Jain A K (2012). Three distinct global estimates of historical land-cover change and land-use conversions for over 200 years. Front Earth Sci, 6(2): 122–139

Meng X L (2010). Multi-scale Relationships Between Impervious Surface, Vegetation, Water and Urban HeatIsland. East China Normal University

Ridd M K (1995). Exploring a V-I-S (vegetation-impervious surface-soil) model for urban ecosystem analysis through remote sensing: Comparative anatomy for cities. Int J Remote Sens, 16(12): 2165–2185

Slonecker E T, Jennings D B, Garofalo D (2001). Remote sensing of impervious surfaces: a review. Remote Sens Rev, 20(3): 227–255

Small C (2001). Estimation of urban vegetation abundance by spectral mixture analysis. Int J Remote Sens, 22(7): 1305–1334

Van De Gfiend A, Owe M (1993). On the relationship between thermal emissivity and the normalized difference vegetation index for nature surfaces. In ternational Journal of Remote Sensing, 14(6): 1119–1131

Weng Q (2012). Remote sensing of impervious surfaces in the urban areas: Requirements, methods, and trends. Remote Sens Environ, 117: 34–49

Weng Q, Liu H, Lu D (2007). Assessing the effects of land use and land cover patterns on thermal conditions using land scape metrics in city of Indianapolis, United States. Urban Ecosyst, 10(2): 203–219

Weng Q, Lu D, Schubring J (2004). Estimation of land surface temperature–vegetation abundance relationship for urban heat island studies. Remote Sens Environ, 89(4): 467–483

Wong N H, Yu C (2005). Study of green areas and urban heat island in a tropical city. Habitat Int, 29(3): 547–558

Xian G, Crane M, Su J (2007). An analysis of urban development and its environmental impact on the Tampa Bay watershed. J Environ Manage, 85(4): 965–976

Xiao R B, Ouyang Z Y, Zheng H, Li E F, Schienke E W Wang X K (2007). Spatial pattern of impervious surfaces and their impacts on land surface temperature in Beijing, China. J Environ Sci (China), 19 (2): 250–256

Xu J H, Ai N S, Chen Y, Mei A X, Liao H J (2003). Quantitative analysis and fractal modeling on the mosaic structure of landscape in the central area of Shanghai metropolis. Chin Geogr Sci, 13(3): 199–206

Xu J H, Lu Y, Ai N S, Yue W Z (2001). A study on landscape mosaic structure in urban-rural area in Northwest of China with RS and GIS. Chin Geogr Sci, 11(4): 366–376

Yang X, Liu Z (2005). Use of satellite-derived landscape imperviousness index to characterize urban spatial growth. Computers, Environment and Urban Systems, 29(5): 524–540.

Yue W (2005). Study on Urban Landscape Pattern and Its Thermal Environment Eeffect Based on Remote Sensing Image. East China Normal University

Yuan F, Bauer M E (2005). Comparison of impervious surface area and normalized difference vegetation index as indicators of surface urban heat island effects in Landsat imagery. Remote Sensing of Environment, 106(3): 375–386.

Yue W (2009). Improvement of urban impervious surface estimation in Shanghai using Landsat7 ETM+ data. Chin Geogr Sci, 19(3): 283–290

Yue W, Liu Y, Fan P, Ye X, Wu C (2012). Assessing spatial pattern of urban thermal environment in Shanghai, China. Stochastic Environ Res Risk Assess, 26(7): 899–911

Zhang Y, Odeh I OA, Han C (2009a). Bi-temporal characterization of land surface temperature in relation to impervious surface area, NDVI and NDBI, using a sub-pixel image analysis. International Journal of Applied Earth Observation and Geoinformation, 11(4): 256–264

Zhang X, Zhong T, Feng X, Wang K (2009b). Estimation of the relationship between vegetation patches and urban land surface temperature with remote sensing. Int J Remote Sens, 30(8): 2105–2118

Zhou S Z, Zhang C (1982). On the Shanghai urban heat island effect. Acta Geographica Sinica, 37(4): 372–381 (in Chinese)

Zhou W, Huang G, Cadenasso M L (2011). Does spatial configuration matter? Understanding the effects of land cover pattern on land surface temperature in urban landscapes. Landsc Urban Plan, 102(1): 54–63